1,3-benzodithiazolium cation **1**[S_2N] also show similar results.[11]

For the phosphorus cations, the calculated HOMO–LUMO and n–π^* separations are largest for **1**[N_2P] and smallest for **1**[S_2P]. While transition energies obtained in this manner are unreliable, on a comparative basis the trend is consistent with the atomic orbital energies of nitrogen and sulfur, the colors of these compounds (**1**[N_2P], colorless; **1**[NSP], pale yellow; **1**[S_2P], yellow-orange), and the UV–visible and MCD spectra of **1**[S_2P] and **1**[NSP].[48] Deviations from naphthalenic character are more prominent in the unoccupied orbitals. Of particular interest are the π-LUMOs, which are essentially identical in form throughout the series and are based primarily at the 2 position (P or CH). Therefore, in contrast to the nitrogen derivative **1**[S_2N],[11] which demonstrates an essentially equal contribution from the sulfur and nitrogen centers in the π-LUMO, nucleophilic attack is expected to predominate at the phosphorus centers of **1**[S_2P], **1**[NSP], and **1**[N_2P]. In addition, the diphosphine **4**, prepared by Baudler from the reaction of **2**[S_2PCl] with sodium,[23a] will be principally P–P σ-bonded, in contrast to the novel π^*–π^* geometry of the nitrogen derivative.[11,50,51]

Anion Basicity and Cation Stability. The identification of the cationic heteronaphthalenic framework **1** as a synthetic template was reliant upon the versatility of the halide abstraction[52] procedure for the preparation of non-metal and organic cations. For systems containing the heavier elements, the stability of the ionic arrangement over an alternative covalent arrangement is dependent upon the low basicity of the anion.[51,53] In contrast, the nitrogen derivative **1**[S_2N] is a stable ionic system as a halide salt.[10,11] The preference for π-bonding between nitrogen and sulfur precludes the formation of a weak N–Cl covalent bond, while the preference for σ-bonding for the heavier elements requires some competition for the chloride ion, by a Lewis acid, in order to stabilize the π-bonded arrangement. Nevertheless, the cations **1** require the inherent stability to avoid other possible disproportionation reactions. The covalent halides **2**[NSPCl] and **2**[NSPBr] exhibit a substantial degree of ionic character in the solid state without the presence of a Lewis acid. On this basis, we may view the derivatives of **1**, **2**, and **3** as a series of Lewis adducts of varying strength.

(1) Compound **3** contains a standard P–C covalent bond and represents the most strongly bound adduct of **1**, with Ph^- as the base (pK_a(benzene) = 43).[54]

(2) The monomeric units of the halide derivatives of **2** have partial ionic character and may be considered as ion-pairs (pK_a(HCl) = −6; pK_a(HBr) = −8).[55] The shorter P–Z covalent bond may be considered as a donation from the halide into the phosphorus-based π-LUMO of the cation from above the plane.

(3) The weakest interactions are observed in the solid-state structures of $AlCl_4^-$ salts of **1**. The long anion/cation contacts (>3.30 Å) are best envisaged as donor/acceptor interactions from the complex anion to the cation. While a number of these contacts take place at the phosphorus center above and below the plane (into π-LUMO), there are numerous in-plane interactions and contacts to the heteroatoms. Also in this category are the long intermonomer contacts observed for **2**[NSPCl] and **2**[NSPBr].

Acknowledgment. We thank the NSERC (N.B. and P.S.W.), the donors of the Petroleum Research Fund, administered by the American Chemical Society (N.B.), and the Killam Foundation (B.W.R.) for financial support, Dr. Kathy V. Darvesh for assistance with molecular orbital calculations, and the reviewers for their comments. All NMR spectra were obtained at the Atlantic Region Magnetic Research Center.

Supplementary Material Available: Tables of crystal data, hydrogen atom coordinates, anisotropic thermal parameters, geometries for molecular orbital calculations, and calculated energies and a unit cell diagram (7 pages); tables of calculated and observed structure factors (37 pages). Ordering information is given on any current masthead page.

(50) Awere, E. G.; Burford, N.; Mailer, C.; Passmore, J.; Schriver, M. J.; White, P. S.; Banister, A. J.; Oberhammer, H.; Sutcliffe, L. H. *J. Chem. Soc., Chem. Commun.* **1987**, 66.
(51) Burford, N.; Passmore, J.; Sanders, J. P. From Atoms to Polymers. In *Molecular Structure and Energetics*; Liebman, J. F.; Greenberg, A., Eds.; VCH: New York, 1989; Vol. 11, p 53.
(52) Olah, G. A.; Kobayashi, S.; Tashiro, M. *J. Am. Chem. Soc.* **1972**, *94*, 7448.
(53) Gillespie, R. J. *Chem. Soc. Rev.* **1979**, *8*, 315.
(54) Steitwieser, A.; Scannon, D. J.; Meimeyer, H. M. *J. Am. Chem. Soc.* **1972**, *94*, 7936.
(55) Perrin, D. D. *Ionisation Constants of Inorganic Acids and Bases in Aqueous Solution*, 2nd ed.; Pergammon Press: Oxford, 1982.

Contribution from the Institut für Physikalische und Theoretische Chemie, University of Erlangen-Nürnberg, D-8520 Erlangen, West Germany, Institut für Heisse Chemie, Kernforschungszentrum Karlsruhe, D-7500 Karlsruhe, West Germany, and Department of Chemistry, The University of New South Wales, Kensington, NSW 2033, Australia

Detailed Hysteresis Studies and Nature of the Spin-State Transition in Bis(1,10-phenanthroline-2-carbaldehyde phenylhydrazone)iron(II) Complexes

E. König,*[1] B. Kanellakopulos,[2] B. Powietzka,[2] and H. A. Goodwin[3]

Received January 2, 1990

An extensive series of scanning curves within the hysteresis loop associated with the spin-state transition in $[Fe(phy)_2](ClO_4)_2$ has been constructed on the basis of magnetic susceptibility measurements (phy = 1,10-phenanthroline-2-carbaldehyde phenylhydrazone). The areas of scanning curves F depend on the temperature width of the curves ΔT and the value of the square of the effective magnetic moment μ_{eff}^2 defined at the center of gravity of the curves. For each value of ΔT, an approximately parabolic relation between log (F/F_{tot}) and log μ_{eff}^2 is found where F_{tot} is the area of the associated hysteresis loop. Similar results have been obtained for the spin-state-transition compound $[Fe(phy)_2](BF_4)_2$. The results for the inner scanning curves do not conform to theorem 4 of the domain theory of Everett. Symmetry relations derived on the basis of simple nucleation (VWBD) theory are not followed. The consequences of these findings are discussed. A linear relation between log (F_{max}/F_{tot}) and the reduced width $\Delta T/\Delta T_{tot}$ has been empirically established where F_{max} is the maximum area of the scanning curves for a particular value of ΔT. The relation has been verified for the right boundary scanning curves of $[Fe(phy)_2]X_2$, X = ClO_4 and BF_4, and $[Fe(bpp)_2](BF_4)_2$ (bpp = 2,6-bis(pyrazol-3-yl)pyridine).

Spin-state transitions in complexes of certain transition-metal ions often proceed as phase transitions of first order.[4] Evidence for the thermodynamic character of the transition is provided by the discontinuous change of entropy (following from calorimetric[5] and DSC measurements[6-8]) and volume (derived from X-ray

(1) University of Erlangen-Nürnberg.
(2) Kernforschungszentrum Karlsruhe.
(3) The University of New South Wales.
(4) König, E.; Ritter, G.; Kulshreshtha, S. K. *Chem. Rev.* **1985**, *85*, 219.
(5) Sorai, M.; Seki, S. *J. Phys. Chem. Solids* **1974**, *35*, 555.

0020-1669/90/1329-4944$02.50/0

diffraction measurements,[9] the second-order Doppler shift of the Mössbauer spectra,[10,11] and Debye–Waller factors). In order to take place at a measurable rate, a first-order transition always requires some degree of superheating or supercooling. The transformation therefore does not occur at the true critical temperature T_c, where the free energies G_{HS} and G_{LS} of the two phases high-spin (HS) and low-spin (LS) are exactly equal, $G_{HS} = G_{LS}$, but rather at the superheating temperature $T_c^{\uparrow} > T_c$ and the supercooling temperature $T_c^{\downarrow} < T_c$. Thus a thermal hysteresis of width $\Delta T_c = T_c^{\uparrow} - T_c^{\downarrow}$ results, which may be considered as a characteristic property of the transition. There are two possible causes for the appearance of such hysteresis: (i) a distribution of transition temperatures as the result of domain formation; (ii) a distribution of nucleation rates as a consequence of kinetic barriers. Domain formation may be studied by application of the model of Everett,[12-14] whereas nucleation rates are governed by VWBD theory.[15,16]

The appearance of *thermal* hysteresis in an electronic-spin-transition system provides a very convenient means for studying such a process. Since the spin transition that accompanies the phase transition results in profound and fundamental changes in the electronic properties of the system, a precise monitoring of the details of the hysteresis behavior becomes feasible. Thus spin-transition systems can provide an ideal model for testing the applicability of Everett's theory to thermal hysteresis. In the Everett model, hysteresis phenomena are described in terms of the behavior of an ensemble of domains under the influence of an independent variable. For spin-state transitions, a domain is formed by a number of complex molecules of like spin, HS or LS. The detailed study of hysteresis effects provides a means for the establishment of the nature of the cooperativity in spin-state transitions. Theorem 4 of the Everett model, which relates to the areas of inner loops of hysteresis (scanning curves), is particularly diagnostic in this respect. According to this theorem, the areas of two scanning curves of an extensive parameter (such $\chi T \sim \mu_{eff}^2$ used here) between the same temperature limits T_A and T_B should be equal,[13] *provided the domains are independent*.[17] The employment of an extensive parameter is a necessary condition of the model of Everett. Thus χ is an extensive parameter and, since the product of an extensive parameter with an intensive parameter (such as T) remains extensive, the product χT has been used here for convenience.

In the first study of scanning curves of the hysteresis associated with a spin-state transition, two such curves were constructed for the complex $[Fe(phy)_2](ClO_4)_2$ (phy = 1,10-phenanthroline-2-carbaldehyde phenylhydrazone).[18] Since the areas of the two scanning curves were found to be equal to within 3%, it was concluded that the transition proceeds via formation of *independent* domains of the two phases HS and LS. Although the two curves contacted the right-hand boundary of the primary hysteresis loop, they did encompass the same temperature limits to within the experimental uncertainty of ±0.2 K and hence the conclusions reached were reasonable. For the spin-state transition in $[Fe(bt)_2(NCS)_2]$(bt = 2,2′-bi-2-thiazoline), Müller et al.[19] observed similar agreement (within 4 ± 1%) for the areas of two scanning curves and concluded that *independent* domains were involved in this transition as well.

Recently, in a detailed study of the hysteresis associated with the spin-state transition in $[Fe(bpp)_2](BF_4)_2$ (bpp = 2,6-bis(pyrazol-3-yl)pyridine), we have demonstrated[20] that theorem 4 of the Everett model is not applicable in this instance and thus independent domains are not formed. For this system, an extensive series of scanning curves was constructed by detailed and accurate measurements of magnetic susceptibility. The curves were of all three types, left boundary, entirely inner, and right boundary. Two series of entirely inner scanning curves were obtained, one spanning the temperature range 174.0–180.5 K (four curves) and the other 173.0–176.0 K (seven curves). Within each series, wide divergence of area was observed. Moreover, the relative area of the curves passes through a maximum if plotted versus the range of magnetic moment squared values covered by the curves. Obviously, in the vicinity of the maximum, areas of scanning curves will not differ very markedly. It follows that the validity of theorem 4 of the Everett model is not necessarily established by consideration of the areas of only a small number (e.g. two) of scanning curves.

In the present contribution, we report the results of an extended study of the hysteresis associated with the spin-state transition in $[Fe(phy)_2](ClO_4)_2$. The study was undertaken to determine whether the earlier results obtained for this system do in fact indicate a difference in the cooperativity of the transition it diplays and the one in $[Fe(bpp)_2](BF_4)_2$. The spin-state transition for the compound $[Fe(phy)_2](ClO_4)_2$ has been thoroughly characterized, the transition temperatures being $T_c^{\uparrow} = 256.1$ K and $T_c^{\downarrow} = 248.0$ K.[18] The features of the hysteresis loop have been established by studies of the temperature dependence of the ^{57}Fe Mössbauer effect, X-ray powder diffraction, and the magnetic susceptibility, the width of the hysteresis resulting as $\Delta T_c = 8.1$ K. The enthalpy and entropy changes at the transition have been determined as $\Delta H = 15.8$ kJ mol^{-1} and $\Delta S = 64.6$ J K^{-1} mol^{-1}, respectively.[8] The spin-state transition in $[Fe(phy)_2](BF_4)_2$ has been similarly characterized,[21] and the details of its hysteresis are also examined in the present work.

Experimental Section

Sample Preparation. The ligand was prepared directly by interaction of 1,10-phenanthroline-2-carbaldehyde with phenylhydrazine in ethanol. The raw product was recrystallized from aqueous ethanol.

The iron(II) complexes were obtained by addition of a solution of the metal salt in hot ethanol to a hot ethanolic solution of the hydrazone.[22] The complexes were washed with ethanol and dried at 60 °C under vacuum. The sample purity was checked by elemental analyses for C, H, N, and Fe and by ^{57}Fe Mössbauer spectroscopy.

Magnetic Measurements. Magnetic susceptibilities were measured with a Faraday-type magnetometer equipped with a custom-made helium/N_2 bath cryostat. The magnetometer employs a 10-in. B-E25C8 electromagnet (Bruker-Physik) with Henry-type pole caps, an electrical microbalance (Sartorius Type 4102), and the required control electronics. Measurement and regulation of sample temperature was achieved by two independent Cu/constantan and Au(Fe)/chromel thermocouples calibrated against a Pt or Ge resistor. The calibration was carefully checked against the inverse magnetic susceptibility of three standard substances that are known to follow rigorously the Curie–Weiss law below 10 K, viz. $FeSO_4 \cdot 7H_2O$, $CuSO_4 \cdot 5H_2O$, and $K_2Ni(SO_4)_2 \cdot 6H_2O$.[23] By use of this procedure, an absolute accuracy of temperature determination of ±0.02 K was achieved between 0.98 and 9.0 K. This calibration was subsequently extended to higher temperatures, thus implicitly assuming validity of the linear $1/\chi_M$ vs T relationship. This assumption was strongly corroborated by measurements of numerous standard substances over an extended period of time. $HgCo(NCS)_4$, $Ni(en)_2S_2O_3$, and $CuSO_4 \cdot 5H_2O$ were used as susceptibility standards.[24] The effective magnetic moment has been obtained according to $\mu_{eff} = 2.828(\chi_M^{cor}T)^{1/2}$, where χ_M^{cor} is

(6) Kulshreshtha, S. K.; Iyer, R. M.; König, E.; Ritter, G. *Chem. Phys. Lett.* **1984**, *110*, 201.
(7) Kulshreshtha, S. K.; Sasikala, R.; König, E. *Chem. Phys. Lett.* **1986**, *123*, 215.
(8) Kulshreshtha, S. K.; Iyer, R. M. *Chem. Phys. Lett.* **1987**, *134*, 239.
(9) König, E. *Prog. Inorg. Chem.* **1987**, *35*, 527.
(10) König, E.; Ritter, G.; Kulshreshtha, S. K.; Nelson, S. M. *J. Am. Chem. Soc.* **1983**, *105*, 1924.
(11) König, E.; Ritter, G.; Kulshreshtha, S. K.; Goodwin, H. A. *Inorg. Chem.* **1983**, *22*, 2518.
(12) Everett, D. H.; Whitton, W. I. *Trans. Faraday Soc.* **1952**, *48*, 749.
(13) Everett, D. H.; Smith, F. W. *Trans. Faraday Soc.* **1954**, *50*, 187.
(14) Everett, D. H. *Trans. Faraday Soc.* **1954**, *50*, 1077; **1955**, *51*, 1551.
(15) Volmer, M.; Weber, A. *Z. Phys. Chem.* **1925**, *119*, 277.
(16) Becker, R.; Döhring, W. *Ann. Phys.* **1935**, *24*, 719.
(17) Enderby, A. *Trans. Faraday Soc.* **1955**, *52*, 106.
(18) König, E.; Ritter, G.; Irler, W.; Goodwin, H. A. *J. Am. Chem. Soc.* **1980**, *102*, 4681.
(19) Müller, E. W.; Spiering, H.; Gütlich, P. *J. Chem. Phys.* **1983**, *79*, 1439.
(20) König, E.; Kanellakopulos, B.; Powietzka, B.; Goodwin, H. A. *Inorg. Chem.* **1989**, *28*, 3993.
(21) König, E.; Ritter, G.; Kulshreshtha, S. K.; Waigel, J.; Goodwin, H. A. *Inorg. Chem.* **1984**, *23*, 1896.
(22) Goodwin, H. A.; Mather, D. W. *Aust. J. Chem.* **1974**, *27*, 965.
(23) König, E. *Landolt-Börnstein, New Series*; Springer: Berlin, 1966; Vol. II/2.
(24) Figgis, B. N.; Lewis, J. In *Technique of Inorganic Chemistry*; Jonassen, H. B., Weissberger, A., Eds.; Interscience: New York, 1965; Vol. 4.

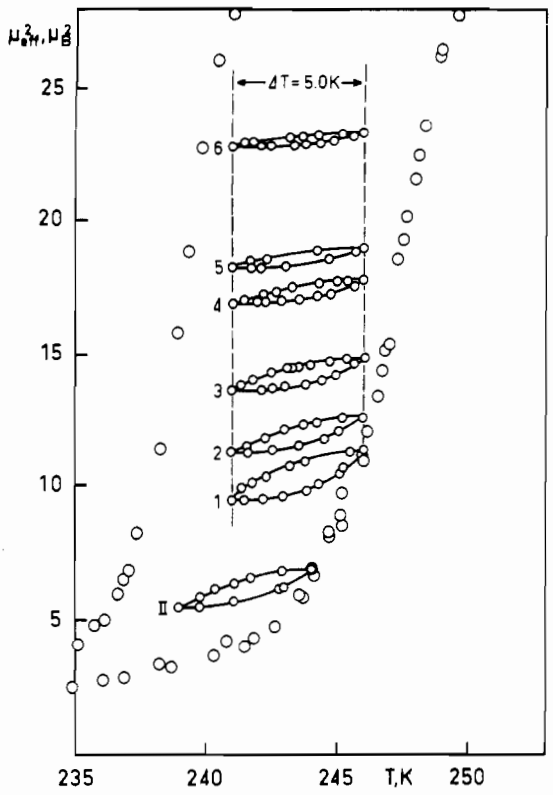

Figure 1. Inner scanning curves of width ΔT = 5.0 K between the temperatures T_A = 241.0 K and T_B = 246.0 K (curves 1–6) within the hysteresis loop of the spin-state transition in $[Fe(phy)_2](ClO_4)_2$. A single right boundary scanning curve (curve II) is also shown.

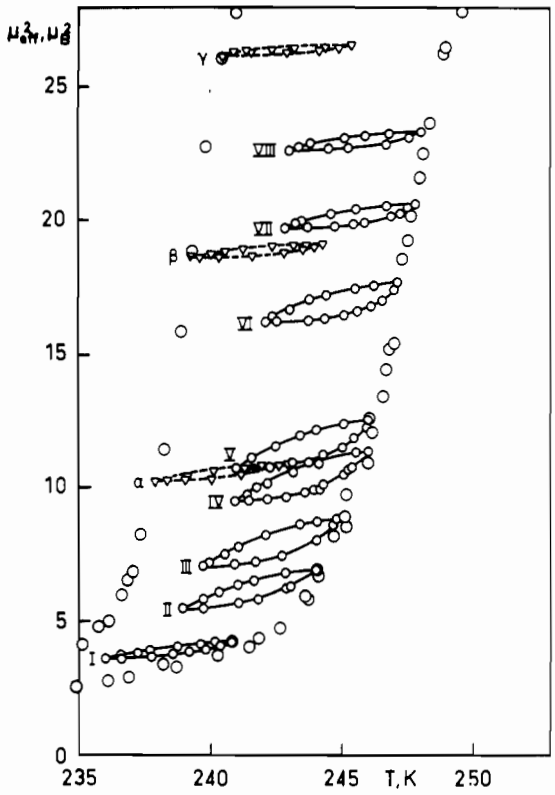

Figure 2. Right boundary scanning curves of width ΔT = 5.0 K with different initial temperatures T_A and final temperatures T_B (curves I–VIII) within the hysteresis loop of the spin-state transition in $[Fe(phy)_2](ClO_4)_2$. Left boundary scanning curves of the same width (curves α, β, γ) are also shown.

the molar magnetic susceptibility corrected for diamagnetism of all constituents and T the temperature in K.

Results

Scanning Curves of $[Fe(phy)_2](ClO_4)_2$. According to measurements of magnetic susceptibility, the effective magnetic moment of the actual sample of $[Fe(phy)_2](ClO_4)_2$ employed in this study varies from μ_{eff} = 5.33 μ_B at 299.7 K, to 0.93 μ_B at 77.7 K, to 0.99 μ_B at 4.20 K. If it is assumed that the limiting values at 299.7 and 4.20 K are due to the pure HS and LS states, respectively, the transition temperature T_c is defined by that value of $\mu_{eff}(T)$ which corresponds to the HS fraction n_H = 0.50 following

$$[\mu_{eff}(T)]^2 = n_H(\mu_{HS})^2 + (1 - n_H)(\mu_{LS})^2 \qquad (1)$$

Thus $T_c^{\uparrow}$ = 246.8 K is obtained for increasing and $T_c^{\downarrow}$ = 239.3 K for decreasing temperatures, a hysteresis loop of width ΔT_c = 7.5 K being formed.

Inner scanning curves of width ΔT = 5.0 K have been measured between the same two temperatures T_A = 241.0 K and T_B = 246.0 K (curves 1–6). These curves are shown in Figure 1. The detailed procedure for this type of measurement has been given by Everett and Smith.[13] In addition, scanning curves contacting the right boundary curve of the hysteresis loop (right boundary scanning curves) with ΔT = 5.0 K but different initial temperatures T_A and final temperatures T_B (curves I–VIII) have been constructed. A similar series of curves contacting the left boundary curve (left boundary scanning curves) with ΔT = 5.0 K (curves α, β, γ) has also been obtained. These two series of curves are displayed in Figure 2. The individual curves are identified, in the figures, by a specific label, their characteristic properties being listed under the same labels in Table I. Furthermore, scanning curves of width ΔT = 6.0 K (curves A–G) and those of width ΔT = 7.0 K (curves a–c) have been measured as right boundary scanning curves. The curves designated by Λ, Δ, Ξ, and Ω in Table I are single scanning curves of specific width ΔT that have not been reproduced in any of the figures. In Figure 3, the reduced area of the right boundary scanning curves is plotted as a function of the effective magnetic moment squared of the particular scanning curve. Each scanning

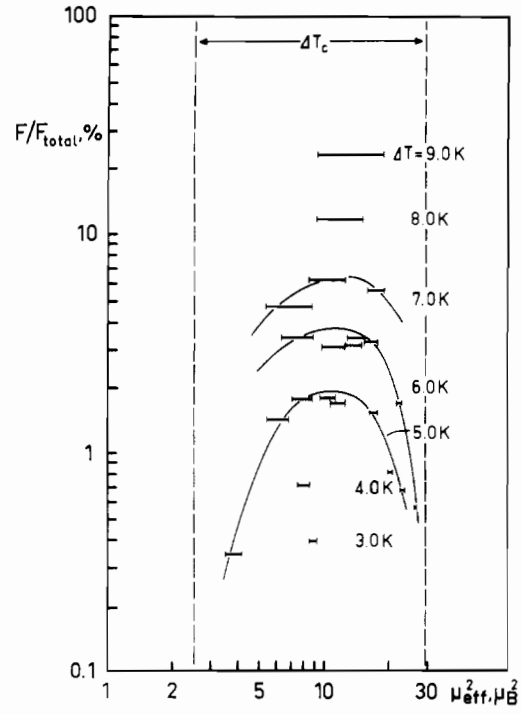

Figure 3. Reduced area of scanning curves F/F_{tot} (in percent) as a function of the effective magnetic moment squared μ_{eff}^2 (μ_B^2) for the spin-state transition in $[Fe(phy)_2](ClO_4)_2$ on a doubly logarithmic scale. F_{tot} denotes the area of the overall hysteresis loop. Bars indicate range of μ_{eff}^2 values covered by a particular scanning curve. Only right boundary scanning curves have been included. Curves order according to the ΔT values 7.0, 6.0, and 5.0 K.

curve is thus represented by a bar that extends over the range of μ_{eff}^2 values covered by that curve. It is seen that the individual scanning curves order on a curve of approximately parabolic shape for each specific value of the temperature range ΔT covered. The

Table I. Characteristic Properties of Scanning Curves of Hysteresis at the Spin-State Transition in $[Fe(phy)_2](ClO_4)_2$

no.	temp, K[a] T_A	T_B	ΔT	μ_{eff}^2, μ_B^2 at T_A	at T_B	area[b]	character of curve
Λ	241.8	244.8	3.0	8.49	9.23	1.69	
Δ	240.8	244.8	4.0	7.45	8.58	3.06	
1				9.40	11.17	7.46	
2				11.17	12.61	5.23	
3	241.0	246.0	5.0	13.57	14.83	5.55	inner sc
4				16.89	17.76	3.20	
5				18.19	18.91	3.67	
6				22.76	23.23	2.01	
I	236.0	241.0	5.0	3.53	4.18	1.48	
II	239.0	244.0	5.0	5.41	6.85	4.83	
III	239.8	244.8	5.0	7.02	8.85	7.50	
IV = 1	241.0	246.0	5.0	9.40	11.17	7.46	right boundary sc
V	241.0	246.0	5.0	10.61	12.43	7.28	
VI	242.1	247.1	5.0	16.23	17.67	6.56	
VII	242.8	247.8	5.0	19.70	20.58	3.45	
VIII	243.0	248.0	5.0	22.55	23.29	2.86	
α	237.9	242.9	5.0	10.20	10.88	1.66	
β	239.2	244.2	5.0	18.55	19.07	1.65	left boundary sc
γ	240.3	245.3	5.0	26.17	26.43	0.86	
A	238.8	244.8	6.0	6.30	8.91	14.64	
B	240.1	246.1	6.0	9.72	12.32	13.20	
C	240.6	246.6	6.0	12.68	15.12	14.12	
D	241.1	247.1	6.0	15.26	17.51	13.95	right boundary sc
E	240.7	246.7	6.0	12.39	14.77	13.24	
F	242.0	248.0	6.0	21.78	22.86	7.20	
G	242.7	248.7	6.0	26.07	26.48	2.39	
a	237.8	244.8	7.0	5.35	8.74	20.23	
b	239.1	246.1	7.0	8.46	12.42	26.40	right boundary sc
c	240.5	247.5	7.0	15.74	18.83	23.77	
Ξ	238.8	246.8	8.0	9.13	14.91	49.5	
Ω	238.4	247.4	9.0	9.18	18.52	99.9	

[a] T_A to T_B is the range of temperatures covered by the particular scanning curve. [b] Area $\mu_{eff}^2 T$ in units of μ_B^2 K.

Table II. Characteristic Properties of Scanning Curves of Hysteresis at the Spin-State Transition in $[Fe(phy)_2](BF_4)_2$

no.	temp, K[a] T_A	T_B	ΔT	μ_{eff}^2, μ_B^2 at T_A	at T_B	area[b]	character of curve
1	277.5	282.0	4.5	8.73	11.27	10.24	inner sc
2				13.21	15.41	9.21	
I	277.5	282.2	4.7	10.02	12.90	12.95	inner sc
II				16.53	18.95	11.65	
A	277.0	282.0	5.0	7.74	10.91	13.94	inner sc
B				12.66	15.23	11.40	
Σ	275.6	283.3	7.7	7.69	23.03	147.6	

[a] T_A to T_B is the range of temperature covered by the particular scanning curve. [b] Area $\mu_{eff}^2 T$ in units of μ_B^2 K.

bars representing the inner scanning curves and those representing the left boundary scanning curves show similar behavior and order below the curve for the right boundary scanning curve. It should be noted that the F/F_{tot} curve representing the inner scanning curves exists only within the interval defined by contact with the parabolas of right and left boundary scanning curves.

Scanning Curves of $[Fe(phy)_2](BF_4)_2$. Magnetic susceptibility measurements on the actual sample of $[Fe(phy)_2](BF_4)_2$ produce values of the effective magnetic moment varying from $\mu_{eff} = 5.27$ μ_B at 310.6 K, to 0.82 μ_B at 77.7 K, to 0.62 μ_B at 4.20 K. For the values at 310.6 and 4.20 K for μ_{HS} and μ_{LS}, respectively, the spin-state transition temperatures are obtained as $T_c^{\uparrow} = 282.4$ K for increasing and $T_c^{\downarrow} = 276.4$ K for decreasing temperatures, the width of the hysteresis loop thus resulting as $\Delta T_c = 6.0$ K.

A pair of inner scanning curves of width $\Delta T = 4.5$ K has been measured between the temperatures $T_A = 277.5$ K and $T_B = 282.0$ K (curves 1, 2). Two additional pairs of inner scanning curves with $\Delta T = 4.7$ K (curves I, II) and with $\Delta T = 5.0$ K (curves A, B) have been also constructured. These curves are shown in Figure 4, their characteristic properties being listed in Table II under the appropriate label. The curve designated Σ is a single scanning curve that has not been reproduced in the figure.

The somewhat different transition temperatures $T_c^{\uparrow}$ and $T_c^{\downarrow}$ for both spin-transition compounds $[Fe(phy)_2]X_2$, X = ClO_4 and BF_4, as compared to the published values[18,21] are not surprising. It has been pointed out previously that details of a spin-state transition may be affected significantly by properties of the particular solid sample.

Discussion

Scanning Curves and the Domain Model of Everett. According to theorem 4 of the Everett model, the areas of the inner scanning curves 1–6 of $[Fe(phy)_2](ClO_4)_2$ (Figure 1), all measured between the same temperatures $T_A = 241.0$ and $T_B = 246.0$ K, should be equal. It is obvious from the figure that this is not the case, the area difference for adjacent curves varying between 0.32 μ_B^2 K, or 6.1%, for curves 2 and 3 and 1.66 μ_B^2 K, or 45.2%, for curves 5 and 6. A more detailed inspection of the areas listed in Table I shows that the values pass over a maximum. The areas of the left or right boundary scanning curves are different from the areas of the inner scanning curves, but they also display, for each particular ΔT range, a similar behavior. This result is illustrated by Figure 3, where the reduced areas of the right boundary scanning curves are plotted, on a logarithmic scale, as a function of the μ_{eff}^2 values covered. According to this presentation, the areas are distributed on a curve of approximately parabolic shape for each particular value of ΔT. The curve for the right boundary scanning curve is always the highest, those for the left boundary and inner scanning curves being somewhat lower. The range of existence of these curves is determined by the μ_{eff}^2 values covered

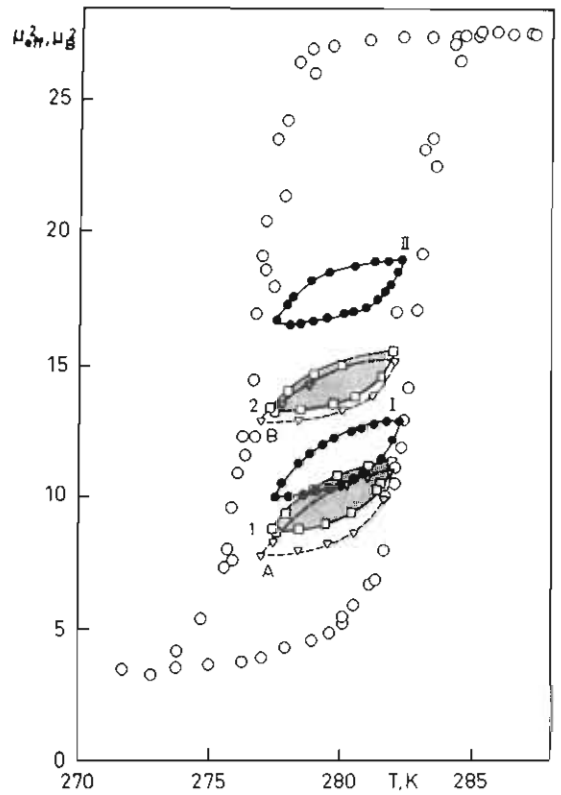

Figure 4. Inner scanning curves of width ΔT = 4.5 K between the temperatures T_A = 227.5 K and T_B = 282.0 K (curves 1, 2 (□), hatched) within the hysteresis loop of the spin-state transition in $[Fe(phy)_2](BF_4)_2$. Inner scanning curves of width ΔT = 4.7 K between T_A = 277.5 K and T_B = 282.2 K (curves I, II (●)) as well as those of width ΔT = 5.0 K between T_A = 277.0 and T_B = 282.0 K (curves A, B (▽)) are also shown.

by the boundary hysteresis curve of the compound, which is indicated in Figure 3 by the broken vertical lines defined by the limiting μ_{eff}^2 values of about 2.5 and 30 μ_B^2.

These results are clearly not consistent with theorem 4 of the domain theory of Everett.[13] According to this theorem, the relative areas of inner scanning curves would have to order, within the presentation of Figure 3, along a horizontal line, and this they obviously do not do. It has been shown that the theorem is applicable only to the case of independent domains.[17] The results are therefore consistent with the assumption that the spin-state transition in $[Fe(phy)_2](ClO_4)_2$ occurs by the conversion of *interacting* domains of like spin. Interaction between different molecules of a spin-crossover compound is required within several theoretical models for these transitions. The interaction may be limited to HS ions, as in the simplified version of an Ising-type model,[25] or comprise the interactions between two HS ions, between a HS and a LS ion, and between two LS ions.[26]

Considering the large differences in area of up to 45%, the previous report[18] of practically equal areas for two scanning curves of $[Fe(phy)_2](ClO_4)_2$ is at first sight surprising. However, inspection of Figure 3 shows that the finding must be fortuitous and must be the result of the range of μ_{eff}^2 chosen for study. Thus, scanning curves situated close to the maximum of one of the parabolic curves will necessarily have similar though not identical areas, whereas the areas of scanning curves located on the slope of one of the parabolas will be significantly different.

For the complex $[Fe(phy)_2](BF_4)_2$, only three pairs of inner scanning curves are available. Nevertheless, the results listed in Table II show trends similar to those described above for $[Fe(phy)_2](ClO_4)_2$. Thus, the areas of each pair of scanning curves show differences between 10.1% for curves 1 and 2 and 18.2% for curves A and B; cf. Figure 4. Clearly, these results are in disagreement with the predictions of theorem 4 of Everett,[13] and thus a significant interaction between domains of this compound may be assumed. The unsuccessful attempt, in a previous study,[21] to obtain reproducible scanning curves for $[Fe(phy)_2](BF_4)_2$ seems to be due to the X-ray powder diffraction method chosen rather than to specific properties of the solid sample, although these cannot be excluded.

Scanning Curves and Nucleation Theory. In general, the predominant component of the activation energy for a phase transformation is associated with the nucleation process, which thus becomes rate determining. Theoretically, the heterogeneous nucleation of solids may be treated largely as an extension of VWBD theory[15,16] which was developed for the homogeneous nucleation of liquid droplets in vapors. Proceeding along similar lines, we may express the number of critical nuclei n_i^* of the parent phase that is formed per unit volume as[27]

$$n_i^* = n \exp[-\Delta G^*/kT] \tag{2}$$

Here

$$\Delta G^* = 16\pi\sigma^3/3(\Delta G_v)^2 \tag{3}$$

is the critical standard free energy (thermodynamic barrier), σ the surface tension, and ΔG_v the bulk free energy decrease per unit volume. The latter may be conveniently expanded, for $|T - T_c| \ll T_c$, in a series as

$$\Delta G_v = (-\Delta S)(T - T_c) + \ldots \tag{4}$$

The nucleation rate R close to T_c may be written as a product of the number of critical nuclei n_i^* and the probability of their conversion to nuclei of the product

$$R = Pn \exp[-\Delta G^*/kT] = (\text{const}) \exp[-B^2/(T - T_c)^2] \tag{5}$$

where $B^2 = 16\pi\sigma^3/3kT_c(\Delta S)^2$. The probability P contains the number of atoms in the interface around the critical nucleus, the vibrational frequency of these atoms, and the probability that the vibration is effected in the direction of the critical nucleus. It follows that R depends only on $|T - T_c|$ and does not differentiate between superheating and supercooling conditions. If the transformation is accompanied by a change of volume ΔV, as is the case for most spin-state transitions,[9] lattice strain will develop. The critical standard free energy then obtains as[28]

$$\Delta G^* = 8\pi^4\mu^2\Delta^4\sigma^3/3(\Delta G_v)^4 \tag{6}$$

where μ is the rigidity modulus and Δ the fractional difference in volume per atom. On the basis of eqs 2 and 4, it follows that R again depends only on the absolute value $|T - T_c|$. If it is assumed that the observed hysteresis associated with a spin-state transition is due to a distribution of nucleation rates, scanning curves should be symmetrically distributed with respect to the point $(T_c; {}^1/_2(n_1 + n_2))$. Here, T_c is the true critical temperature, which may be approximated by the experimentally accessible value $\bar{T}_c = {}^1/_2(T_c^{\uparrow} + T_c^{\downarrow})$, n_1 and n_2 being the HS fractions of the initial and final phases. For $[Fe(phy)_2](ClO_4)_2$, $\bar{T}_c \simeq 243$ K, whereas ${}^1/_2(n_1 + n_2)$ may be represented by $\mu_{eff}^2 \simeq 16.0\ \mu_B^2$. There are no scanning curves available with complete inversion symmetry of their positions, but some are almost so. Thus, the positions of curves VII and α (cf. Figure 2) are close to the symmetry requirement, though their areas (3.45 versus 1.66 μ_B^2 K) are significantly different as are their forms. For $[Fe(bpp)_2](BF_4)_2$, we obtain[20] $\bar{T}_c \simeq 176.7$ K, ${}^1/_2(n_1 + n_2)$ being represented again by $\mu_{eff}^2 \simeq 16.0\ \mu_B^2$. Here, likewise, only approximately corresponding scanning curves have been constructed. However, curves 1 and 4 are almost symmetrically disposed, their areas being 9.73 and 4.26 μ_B^2 K, respectively. In addition, curve 4 may be set against curve α, where the areas have been determined as 4.26 and 2.73 μ_B^2 K, respectively. It is obvious that the expected symmetry relation cannot be established. It should be noted that, on the

(25) Zimmerman, R.; König, E. *J. Phys. Chem. Solids* **1977**, *38*, 779.
(26) Rao, P. S.; Ganguli, P.; McGarvey, B. R. *Inorg. Chem.* **1981**, *20*, 3682.
(27) Turnbull, D. *Solid State Phys.* **1956**, *3*, 225.
(28) Nabarro, F. R. N. *Proc. R. Soc. London* **1940**, *A175*, 519.

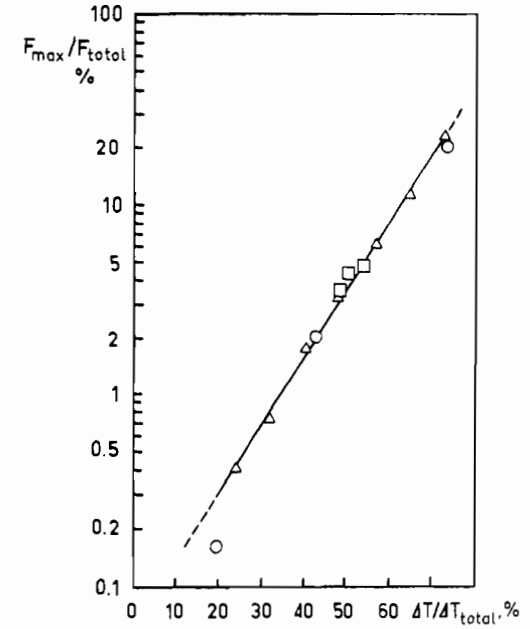

Figure 5. Ratio of the maximum area F_{max} of right boundary scanning curves and the area F_{tot} of the hysteresis loop (on a logarithmic scale) as a function of the reduced width of the scanning curves, $\Delta T/\Delta T_{tot}$. Here the maximum area F_{max} is situated on the plateau of the parabolic curve $\log (F/F_{tot}) = f(\log \mu_{eff}^2)$ such as displayed in Figure 3 and ΔT_{tot} is the width of the overall hysteresis loop as defined in Figure 6. Different signs refer to scanning curves of different spin-transition compounds studied: $[Fe(phy)_2](ClO_4)_2$ (Δ); $[Fe(phy)_2](BF_4)_2$ (□); $[Fe(bpp)_2](BF_4)_2$ (○).

basis of eq 6, the strains that develop for transformations involving a sizable change of volume ΔV will have the consequence that nucleation barriers ΔG^* may be different in the forward and reverse directions. Moreover, Rao and Rao[29] expect that even the transition temperatures T_c may assume different values in the two directions. In both cases, the inversion point would be considerably displaced from the values derived above. From Figure 3 it may be seen that, for the right boundary scanning curves of $[Fe(phy)_2](ClO_4)_2$, the areas are distributed symmetrically with respect to $\mu_{eff}^2 \simeq 12\ \mu_B^2$. For the right boundary scanning curves of $[Fe(bpp)_2](BF_4)_2$, this symmetry arises for $\mu_{eff}^2 \simeq 12\ \mu_B^2$ as well and for the inner scanning curves for $\mu_{eff}^2 \simeq 8\ \mu_B^2$.[20] The inversion point of scanning curves is thus somewhat displaced as compared to the center of μ_{eff}^2 values. For the sake of clarity, inner and left boundary scanning curves have been omitted from Figure 3, but it is found that these order below the right boundary scanning curves, as has been illustrated previously for $[Fe(bpp)_2](BF_4)_2$.[20] Since the areas are decreasing from right boundary over inner to left boundary scanning curves, it is difficult to decide whether there is any inversion symmetry with respect to the transition temperature T_c.

A General Empirical Relation. In Figure 5, the maximum values of the reduced area of right boundary scanning curves F_{max}/F_{tot} are plotted, on a logarithmic scale, as a function of the reduced width of these curves, $\Delta T/\Delta T_{tot}$. The area ratios F_{max}/F_{total} have been extracted from the plateaus of the parabolic curves such as those in Figure 3. The widths of the overall hysteresis loops ΔT_{tot} have been determined by linear extrapolation of the boundary curves following Figure 6. Thus the right boundary is extrapolated to the μ_{eff}^2 value corresponding to the HS fraction $n_{HS} = 1.0$ and the left boundary to the μ_{eff}^2 value corresponding to $n_{HS} = 0$. This definition of ΔT_{tot} is required in order to normalize the width ΔT of the individual scanning curves. It is evident that the logarithm of the area ratio F_{max}/F_{tot} is a linear function of $\Delta T/\Delta T_{tot}$ over a large part of the hysteresis loop and is well represented by

$$\log (F_{max}/F_{tot}) = 0.0379\Delta T/\Delta T_{tot} - 1.350 \qquad (7)$$

(29) Rao, C. N. R.; Rao, K. J. *Phase Transitions in Solids*; McGraw-Hill: New York, 1978.

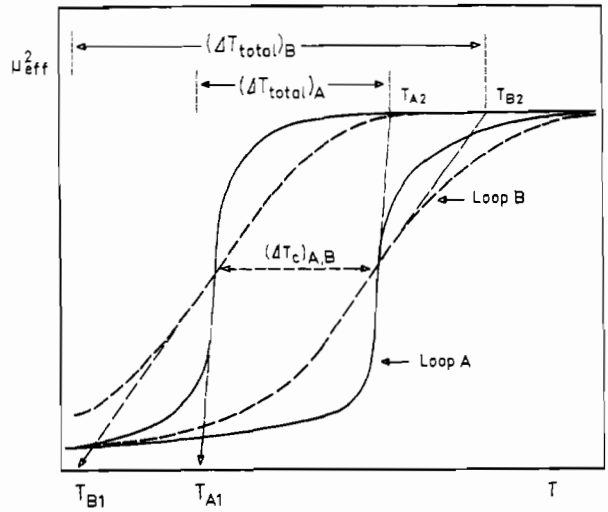

Figure 6. Schematic to illustrate definition of width ΔT_{tot} of the overall hysteresis loop by extrapolation of boundary curves. Determination of ΔT_{tot} for two hysteresis loops of different steepness, A and B, is shown. Thus $(\Delta T_{tot})_A = T_{A2} - T_{A1}$ and similarly for B.

where the percentage error of the coefficients as given by the numerical fit is ±5%. Figure 5 summarizes the results for three spin-state-transition compounds studied thus far. With respect to $[Fe(phy)_2](ClO_4)_2$, it should be noted that only the data points for the widths $\Delta T = 5.0$, 6.0, and 7.0 K have been derived from a larger series of scanning curves and thus should well represent the situation of the plateau. The data points for $\Delta T = 3.0$, 4.0, 8.0, and 9.0 K are derived from a single scanning curve. From Figure 3 it may be observed, however, that the maxima of the parabolic curves arise for almost identical values of μ_{eff}^2. It is seen further that the bars representing the μ_{eff}^2 values which are covered by these scanning curves are situated close to the expected maxima. Thus, it seems that even the data points representing the single scanning curves are suitable for being included into the plot of Figure 5, although a slight uncertainty with respect to the position of these points in the diagram remains. For $[Fe(phy)_2](BF_4)_2$, only two inner scanning curves are available for each of the three widths $\Delta T = 4.5$, 4.7, and 5.0 K. From the data of Table II, it is seen that these curves in fact relate to μ_{eff}^2 values close to the expected maxima of the parabolic curves. In addition, it may be assumed that the maxima of inner scanning curves are not too different from the maxima of corresponding right boundary scanning curves. The three points within Figure 5 thus seem to be reasonably placed. For $[Fe(bpp)_2](BF_4)_2$, the points for $\Delta T = 3.0$ and 6.5 K have been derived from a series of scanning curves and thus should represent the maxima of the parabolic curves reasonably well. Although the point for $\Delta T = 11.2$ K derives from a single scanning curve, inspection of the corresponding parabolas[20] shows that the μ_{eff}^2 values covered are again within the range expected for the maximum. The relationship expressed in Figure 5 has been verified so far for only three spin-state-transition systems for which a detailed analysis of the hysteresis is now available, i.e. $[Fe(phy)_2]X_2$, X = ClO_4 and BF_4, and $[Fe(bpp)_2](BF_4)_2$.[20] Its validity in these three distinct instances does suggest, however, that it may be applicable to the determination of the maximum area of a scanning curve of given width ΔT for any spin-state-transition system of known characteristics, namely area and T_c of the associated hysteresis loop. Unfortunately, attempts at derivation of the empirically established relation from either the domain model of Everett or the nucleation theory have not been successful.

It is obvious that the study of further suitable systems is required to clarify these points and to establish the applicability of the findings to thermal hysteresis behavior in general.

Acknowledgment. We appreciate financial support from the Deutsche Forschungsgemeinschaft, Bonn.

Registry No. $[Fe(phy)_2](ClO_4)_2$, 69746-28-7; $[Fe(phy)_2](BF_4)_2$, 53261-61-3.